COO-3158-71

MASTER

THE SPATIAL DISTRIBUTION OF SELF-INTERSTITIAL ATOMS AROUND DEPLETED ZONES IN TUNGSTEN ION-IRRADIATED AT 10 K

by

Ching-Yeu Wei and David N. Seidman

Cornell University

Ithaca, New York 14853

June 1980

Report #4088

Issued by

The Materials Science Center

Prepared for

THE U.S. DEPARTMENT OF ENERGY UNDER CONTRACT

No. DE-AS02-76ER03158.

DISCLAIMER

THE SPATIAL DISTRIBUTION OF SELF-INTERSTITIAL ATOMS AROUND DEPLETED ZONES IN TUNGSTEN ION-IRRADIATED AT 10 K†

by

Ching-Yeu Wei* and David N. Seidman
Cornell University, Bard Hall, Department of Materials Science and Engineering and the Materials Science Center, Ithaca, New York 14853 U.S.A.

ABSTRACT

The three-dimensional spatial distribution of self-interstial atoms (SIAs) around depleted zones (DZs), in ion-irradiated tungsten, was determined by field-ion microscopy (FIM). High-purity, four-pass zone-refined crystals, tungsten FIM specimens were irradiated in situ with 30 keV Cr^+ or 18 keV Au^+ ions along the $[\bar{7}4\bar{1}]$ direction, at 10 K, and examined at this temperature by the pulse field evaporation technique. At 10 K the SIAs, in tungsten, were completely immobile. The distances were measured, along the close-packed crystallographic directions--that is, the <100>, <110> and <111>-type direction--between each SIA and the DZs. Distance measurements were also made between each SIA and the irradiated surface of the specimen. The set of distances employed for analysis corresponded to the minimum measured distances; thus, the histograms of the distances presented represented a lower bound (denoted by R_{min}) to the actual propagation distances. For the 30 keV Cr^+ ion-irradiated specimen a total of 97 SIAs were detected and $\langle R_{min} \rangle$ was 175 ± 110 Å; the ± values for $\langle R_{min} \rangle$ represent one standard deviation. In the case of the 18 keV Au^+ irradiated specimen the quantity $\langle R_{min} \rangle$ was 175 ± 130 Å; 33 SIAs were detected. A composite distribution of R_{min} values was obtained by combining our earlier measurements (Beavan, Scanlan and Seidman 1971) with the present results to obtain $\langle R_{min} \rangle \simeq 160 \pm 120$ Å. It was suggested that this value may have represented an overestimate of the mean range of replacement collision sequences in tungsten. Nevertheless, the results constituted very direct evidence for the existence of RCSs in tungsten.

---

† This work was supported by the United States Department of Energy. Additional support was received from the National Science Foundation through the use of the technical facilities of the Materials Science Center at Cornell University.

* Now at the General Electric Corporate Research and Development Laboratory, Schenectady, New York 12301, U.S.A.

§1. INTRODUCTION

For over two decades the subject of focused collision sequences (FCSs) and replacement collision sequences (RCSs), in the field of radiation damage, has evoked a great deal of theoretical and experimental research. The start of this subject dates from the seminal paper of Silsbee (1957), in which he introduced the concept of an FCS or focuson in an irradiated crystal lattice. The existence of FCSs provided a mechanism for the efficient transport of momentum along close-packed crystallographic directions without the permanent displacement of lattice atoms. Shortly thereafter Vineyard and co-workers (Gibson et al. 1960, Vineyard 1963, Erginsoy, Vineyard and Englert 1964 and Erginsoy, Vineyard and Shimuzu 1965) in a series of epoch making papers employed the molecular dynamics computer technique to simulate low-energy radiation damage events. The Vineyard et al. computer experiments showed the existence of FCSs and a new type of focused event that is now called an RCS; RCSs were "observed" in both the face-centered (copper) and body-centered (α-iron) cubic crystal lattices. An RCS involves the transport of mass as well as momentum along close-packed crystal lattice directions. As a result of this mechanism it is possible to dynamically produce a self-interstitial atom (SIA) a number of interatomic distances away from its vacancy. Seeger (1958, 1962) also postulated the concept of a dynamic crowdion--RCS in our vernacular--as a means of separating the SIAs from their vacancies in a displacement spike (Brinkman 1954). Both FCSs and RCSs are low-energy phenomena (typically less than one keV of transferred erergy) and they have been discussed extensively as one of the important factors that determine the initial spatial arrangement of vacancies and SIAs in irradiated crystals (for examples, see Thompson 1969 and Nelson 1968); that is, the spatial arrangement prior to the start of extensive thermally activated migration of point defects. Unfortunately, the direct experimental measurement of the mean range and range distribution of either FCSs or RCSs has proved to be a major scientific problem. For example, different types of experiments--on gold--have been interpreted as indicating a mean range of

less than 50 Å (Ecker 1974) and greater than 2000 Å (Seeger 1970). Various aspects of the complex experimental situation have been reviewed by Venables (1970), Blewitt, Kirk and Scott (1975) and Thompson (1978). Also, recently, Tenenbaum and Doan (1977) and Tenenbaum (1978) have employed the molecular dynamics computer technique to calculate the effects of lattice thermal vibrations on RCSs. Despite all this time and effort the subject of FCSs and RCSs has remained extremely controversial.

Tungsten is an interesting element to study in the search for SIAs produced by RCSs, as it is a heavy element with a reasonably large atomic radius; therefore, one would expect focusing effects to be important in its lattice (for example, see Thompson 1969 and Nelson 1968). In this paper we have presented new results on the spatial distribution of SIAs around depleted zones (DZs)†, created as the result of in situ irradiations--of tungsten field-ion microscope (FIM) specimens at 10 K--with 30 keV Cr^+ or 18 keV Au^+ ions. At 10 K, in tungsten, we have demonstrated that the SIAs were completely immobile (Scanlan, Styris and Seidman 1971a and 1971b, Seidman, Wilson and Nielsen 1975a and 1975b, Wilson and Seidman 1975 and Wilson, Baskes and Seidman 1980). The experimental approach was similar to the one we employed in an earlier piece of research (Beavan, Scanlan and Seidman 1971), although the FIM techniques have been refined considerably since that publication (Seidman 1978). The basic procedure was to dissect a specimen at 10 K, after an in situ irradiation, on an atom-by-atom basis to search for both the DZs and SIAs. Thousands of FIM images were recorded on 35 mm ciné film, which were subsequently analyzed to determine the three-dimensional spatial relationships between the DZs and SIAs. This procedure enabled us to determine the distances, along the close-packed crystallographic directions, between each SIA and the DZs. Distance measurements were also made between each SIA and the irradiated surface of the specimens. The set of distances employed for the analysis corresponded to the minimum measured distances -- denoted R_{min}. For the 30 keV Cr^+ ion-irradiated specimens a total of 97 SIAs were detected and $\langle R_{min} \rangle$ was 175 ± 110 Å. In the case of the 18 keV Au^+ irradiated specimen the value of $\langle R_{min} \rangle$ was 175 ± 130 Å. A composite

† We have used this term--in preference to displacement spike--to refer to a region of high vacancy concentration after all the deposited energy, both elastic and inelastic, has been dissipated.

distribution of R_{min} values was obtained by combining our earlier measurements (Beavan et al. 1971) for 25 SIAs with the present results; for this composite distribution $\langle R_{min} \rangle$ was $\simeq 160 \pm 120$ Å. It was concluded that this value of $\langle R_{min} \rangle$ most likely represented an overestimate of the mean range of RCSs in tungsten. However, the results do constitute firm evidence for the existence of RCSs--in tungsten--but the exact relationship between the distributions we measured and the parent standard distribution is unknown at present.

§2. EXPERIMENTAL DETAILS

2.1. Specimen Chemistry and Preparation

Four pass zone-refined single crystal rods 1.0 to 1.5 mm in diameter and 20 cm in length were prepared by the electron beam zone-melting technique. They were first reduced to a 0.5 mm diameter rod by electropolishing at 30 Vdc in a solution of 20 g NaOH in one liter of a 60-40 mixture of glycerol and water, with air bubbled through the electrolyte. The thinned rods were then polished and sectioned into 2 cm lengths (0.1 mm diameter) in a 1 N NaOH electrolyte at 9 Vdc. A section of the rod specimen was mounted in a specimen holder and polished to a sharply-pointed FIM tip by the ac drop-off technique (Müller and Tsong 1969). The specimen was immersed vertically into a layer of 1 N NaOH aqueous solution which was floated on top of CCl_4. A 4 Vac potential was then applied between the specimen and a stainless steel counter electrode until a slightly necked region was produced at the interface between the NaOH and CCl_4. The specimen was next raised slightly and the neck was allowed to propagate inward until the lower section of the wire dropped off. At this point the specimen had a thin and long taper. It was polished again by the procedure described above, but before the lower section of the wire dropped off the voltage was switched to an $\sim$3 Vac pulse controlled by a momentary push-button switch. The pulse was terminated when the lower section was observed to drop into the solution. A specimen produced by this ac drop-off technique imaged at a potential of 3 to 4 kV in the FIM; this corresponded to a tip radius of $\sim$100 Å. The initial end-form of the electropolished tip was extremely rough on an atomic scale. An atomically smooth end-form was obtained by combining dc and pulse field-evaporation at 78 K.

2.2. The Irradiation Procedure

After a specimen had been field evaporated to a tip radius of 200 to 400 Å, it was cooled to 10 K and brought to an atomically smooth low-temperature end-form by the pulse field evaporation technique. The specimen was irradiated *in situ* at a background pressure $\leq 2 \times 10^{-9}$ torr--in the absence of the electric field and imaging gas--with a magnetically-analyzed 30 keV Cr^+ ion beam to a total dose of 4×10^{12} ions cm^{-2}. The flux of ions at the specimen was $\sim 10^{11}$ cm^{-2} sec^{-1}. A second specimen was irradiated with a magnetically-analyzed 18 keV Au^+ ion beam to a total dose of 5×10^{13} ions cm^{-2}; the flux of ions at this specimen was $\sim 2 \times 10^{12}$ cm^{-2} sec^{-1}. In both cases the time required to form an adsorbed monolayer was always greater than the irradiation period. After a 10 K irradiation each specimen† was re-imaged, employing helium as the imaging gas, at $\sim 1 \times 10^{-4}$ torr. Each specimen was dissected atom-by-atom employing the pulse field evaporation technique (Seidman 1973, 1976, 1978 and Seidman, Wilson and Nielsen 1975a and 1975b).

For details regarding temperature control and measurement, the sputtered-metal ion-source and the irradiation facility see Seidman *et al*. 1969, Seidman and Scanlan 1971, Scanlan *et al*. 1971a, Pétroff and Seidman 1973 and Wilson and Seidman 1975.

2.3. Data Recording System and Ciné Film Analyzer

An FIM image was recorded photographically after a field-evaporation pulse had been applied; the pulse height and duration were adjusted so that one atom, on the average, was removed per pulse on the (222) plane. The FIM images were recorded on 35 mm ciné film employing an Automax ciné camera equipped with a 1000 foot film chamber. The 35 mm ciné film was analyzed with a Vanguard motion analyzer which was interfaced to a Houston Omnigraphic 200 x-y recorder; see our earlier publications for further details (Scanlan *et al*. 1969, Beavan *et al*. 1971, Wilson and Seidman 1973, Seidman 1976 and Wei and Seidman 1978).

---

† At 10 K we have demonstrated that SIAs were immobile (Scanlan, Styris and Seidman 1971a and 1971b, Seidman, Wilson and Nielsen 1975a and 1975b, Wilson and Seidman 1975 and Wilson, Baskes and Seidman 1980).

§3. CONTROL EXPERIMENTS

Control experiments were performed on unirradiated tungsten specimens to detect possible artifact vacancies and SIAs. The term artifact vacancy or SIA implied the presence of a vacancy or an SIA which was not the result of an irradiation. A vacancy appeared as a dark spot at the position of an atomic site. It has been shown that an SIA can produce a contrast pattern (Seidman and Lie 1972) consisting of: (a) a bright spot; (b) an extra bright-spot and (c) a vacant lattice site.

The criteria employed for counting both atomic sites and vacancies were as follows: (1) for small net planes (<20 atoms) we counted both atomic sites and vacancies within the first ring of atoms (see fig. 1) immediately after the last atom of the preceding plane had been field-evaporated; and (2) for large net planes (≥20 atoms) we counted both atomic sites and vacancies within the first ring when the first two outer rings of atoms had become visible, even though several atoms of the preceding plane were still retained. Figure 1 shows a schematic diagram of an (hkl) net plane. The solid-black circles represent atoms and the open circles represent vacancies. The first ring is indicated by the solid line and only atomic sites that were contained within the solid line were counted. In fig. 1 there were two vacancies, as indicated by the numbers 4 and 5, and the total number of atomic sites was 16. The vacancies denoted by the numbers one to three on the first ring may have been created as a result of an irregular field-evaporation sequence at the edge of the plane. In practice the artifact vacancy concentration in the first ring of atoms was found to be high and it was also difficult to measure, therefore the artifact vacancy concentrations reported in this section did not include the vacancies which appeared in the first ring of a net plane.

Five families of vicinal planes near the (222) pole--that is, the {222}, {332}, {443}, {442}, and {543} planes-- and eight families of planes near the (411) pole--that is, the {411}, {521}, {622}, {631}, {721}, {732}, {831} and {842} planes--were examined by the pulse field evaporation technique. In a grand total of 10^5 atoms counted in the five families of vicinal planes near the (222) pole we found no evidence

of artifact vacancies or SIAs; the artifact vacancy and SIA concentrations for these planes was therfore $<1\text{x}10^{-5}$ at.fr. More extensive control experiments on pure tungsten by the pulse field evaporation experiment were performed by Park (1975); he also found that for the vicinal planes near the (222) pole the artifact vacancy concentration was $<\sim 1\text{x}10^{-5}$ at.fr.*

No artifact vacancy or SIA concentration measurements have been reported for the planes near the (411) pole and therefore we examined them extensively in our work. The total number of atoms and artifact vacancies counted for each plane are listed in Table 1. In most cases the artifact vacancy concentration was between $1\text{x}10^{-4}$ and $1\text{x}10^{-3}$ at.fr. with the exception of the {622} planes. In addition, no contrast patterns of SIAs were detected among a total of $\sim 7\text{x}10^{5}$ atomic sites counted in these studies; hence, the artifact SIA concentration for the planes near the (411) pole was $<1.4\text{x}10^{-6}$ at.fr. In conclusion, the results presented in this paper were <u>not</u> affected by the presence of artifact SIAs or vacancies.

§4. RESULTS

4.1. The 30 keV Cr^{+} Ion Irradiation

In one specimen which had been irradiated with 30 keV Cr^{+} ions we found five depleted zones (DZs)† and a total of 97 SIAs in the lattice surrounding these DZs; the SIA concentration was $\sim 9\text{x}10^{-5}$ at.fr. Figure 2a exhibits a partial 121 standard stereographic projection which shows a top view of the specimen; this specimen had a [121]

---

* In a total number of $\sim 1\text{x}10^{6}$ atomic sites counted in two well-annealed pure tungsten specimens Park (1975) found only one β-dark spot contrast effect; a β-dark spot was a single dark-spot that appeared <u>suddenly</u> within a well-resolved net plane during observation and remained there until all the atoms of that plane had been field evaporated. This β-dark spot contrast effect, however, was <u>not</u> counted as a vacancy in our work. The origin of this contrast effect was most likely a result of the interaction of the imaging gas with the atoms in the surface of the specimen.

† In only one out of the four tungsten specimens which had been irradiated with 30 keV Cr^{+} ions did we find DZs which were capable of being mapped with atomic detail; they were denoted as DZ5a and DZ5b. The results on the vacancy structure of these depleted zones will be reported separately (Wei, Current, and Seidman 1980).

orientation and the ion beam was parallel to the $[\bar{7}4\bar{1}]$ direction. Since the ion beam was parallel to this very high index crystallographic direction the probability of channeling was minimized (for example, see Whitton 1973). The plane (or planes) in which a depleted zone was detected is also indicated; for example, DZ5b was found near the (222) plane of the specimen. A cross-sectional side view of the specimen is shown in fig. 2b. The distance between any two DZs was indicated by the letters a, b, etc.; the distances ranged from 160 to 370 Å.

Figure 3 exhibits a pulse dissection sequence through a typical SIA contrast pattern detected in this specimen. This SIA contrast pattern extended through six (732)* planes and a total of 140 frames of ciné film were involved in the analysis of this contrast pattern; only 12 micrographs are presented in fig. 3 for the sake of clarity. The (732) plane and the surrounding planes are indexed in frame 1; the frame number of the ciné film is located in the lower right-hand corner below each micrograph. The layer number is indicated by the letter n in the upper left-hand corner above each micrograph. Thus, for example, frame 1 corresponds to the n=1 layer and frame 16 to the n=2 layer. The positions of the atoms in the (732) plane are indicated schematically below each micrograph by solid-black circles; a vacancy is indicated by an open circle. Frame 1 shows an atomically perfect plane in layer 1. Layers 2 and 3 (see frames 16 and 30) exhibited two vacancies, respectively. It is noted that frame 30 also shows a bright-spot contrast effect (denoted by ⊛). In layer 4 (frame 52) a weak atomic contrast effect (denoted by ⊛) was seen to appear in a non-lattice site. This extra bright-spot contrast effect increased in size and brightness as the n=4 layer was disected (see frames 52, 56 and 57) and it finally was field evaporated between frames 57 and 64. Frames 64, 83 and 100, which exhibit layers 5, 6 and 7, were observed to contain three vacancies. Finally the n=8 layer shown in frame 122 was seen to be perfect.

---

* This corresponded to a distance of 2.41 Å. The crystallography of the (732) plane was given in Nicholas' atlas (Nicholas 1965).

Figure 4 exhibits a second example of the contrast pattern of an SIA. This SIA contrast pattern extended through six (521) planes* and a total of 581 frames of ciné film were involved in this analysis; only 12 frames of film were exhibited in fig. 4. Layer numbers 4, 5, 6 and 7 (see frames 239, 300, 358 and 403) contained six vacancies. An extra bright-spot contrast effect was also seen in a non-lattice site in layer 5 (see frames 312, 337 and 345). Therefore, an SIA can produce a contrast pattern consisting of: (1) a bright spot; (2) an extra bright-spot; and (3) a vacant lattice site (Seidman and Lie 1972). This type of contrast pattern was only observed in the irradiated specimens and therefore was not caused by artifacts (see §3).

A computer generated isometric drawing of the 30 keV Cr^+ irradiated specimen is shown in fig. 5. The five open ellipses represent the depleted zones (DZ5a to DZ5e) and the solid-black circles represent the SIAs. The mathematical details of the mapping procedure were given in Appendix B. It is noted (see fig. 5) that the DZs were located mainly on the incident-beam side of the specimen, whereas a large fraction of the total number of SIAs observed were detected on the side of the specimen shielded from the Cr^+ ion beam. The clear separation between the DZs and SIAs is evident in fig. 5.

The distances were measured--along the close-packed directions (i.e., the <100> <110> and <111>-type directions)--between each SIA and the depleted zones (DZ5a to DZ5e); it was required that a close-packed direction intersect the cross-sectional area of a DZ. If no close-packed direction was found that connected an SIA to a DZ then the distance was measured along a vector that originated at an SIA and terminated in the center of a DZ. The distances between each SIA and the surface of the specimens, on the irradiated side, were also measured along all the possible <100>, <110> and <111> directions. The distances were measured along close-packed directions, as they

---

* This corresponded to a distance of 3.47 Å. The crystallography of the (521) plane was not given in Nicholas' atlas (Nicholas 1965), so we have presented the details concerning this plane in Appendix A.

were the ones along which the RCSs were most likely propagated (Gibson et al. 1960, Erginsoy et al. 1964 and 1965). Distance measurements were also made between the SIAs and the surface of the specimen--on the irradiated side--because a DZ may have gone undetected if it was located on the periphery of the FIM image near the shank of the specimen. For these two general classes of measured distances we do not know, of course, along which specific vector an individual SIA had been propagated when it was in its dynamic state. In view of this situation we have taken the set of distances which corresponded to the minimum measured distances; thus, the distances presented represented a lower bound--denoted R_{min}--to the actual propagation distances. Figure 6 is a histogram of the number of SIAs per 50 Å; the ± values for $\langle R_{min} \rangle$ represent one standard deviation (σ_m). It is emphasized very strongly that this histogram may not represent the actual distribution of RCS ranges (see §5), although it does provide strong evidence for the existence of RCSs.

4.2. The 18 keV Au^+ Irradiation

In a specimen which had been irradiated with 18 keV Au^+ ions we detected a total of 33 SIAs; all of the depleted zones produced were located within ≤30 Å from the irradiated surface. The value of 18 keV and the heavy mass (196.967 amu) of the projectile ion were chosen so that all of the DZs were created at or slightly below the irradiated surface. The ion beam was parallel to the very high index $[\bar{7}4\bar{1}]$ direction, so once again the probability that the incident ion beam became channeled was negligible (Whitton 1973). This spatial arrangement of DZs implied that the distance from an SIA to a DZ was almost equal to the distance from an SIA to the irradiated surface.

A computer-generated isometric drawing of the specimen which had been irradiated with 18 keV Au^+ ions is shown in fig. 7.* The SIAs that were injected into the bulk of the specimen are indicated by the solid-black circles; the DZs are denoted schematically by the open ellipses. The distances between each SIA and the surface of the specimen were measured along all the possible <100>, <110> and <111>-type directions.

---

* In this drawing the positions of the DZs are simply schematic. For the detailed vacancy structure of the DZs see Wei, Current and Seidman (1980).

In this case we also took the set of distances which corresponded to the minimum measured distances as R_{min} (see §4.1.). Figure 8 presents a histogram of the number of SIAs per 50 Å bin versus R_{min}. The quantity $\langle R_{min} \rangle$ was 175 ± 130 Å, where the ± values were for one σ_m. This value was in good agreement with the value of 175 ± 110 Å measured for the 30 keV Cr^+ ion irradiation.

§5. DISCUSSION

5.1. The Number of SIAs Detected

The total number of SIAs detected in both specimens was always less than the total number of vacancies measured. In the case of the 30 keV Cr^+ ion irradiation we determined experimentally that DZ5a and DZ5b contained 241 and 247 vacancies, respectively (Wei 1978 and Wei, Current and Seidman 1980). It was not found possible to measure the number of vacancies contained within DZ5c to DZ5e but an average value of ∿200 vacancies per DZ for the 30 keV Cr^+ ion irradiations was found to be a reasonable number (Wei 1978, Wei and Seidman 1979). Thus the fraction of SIAs detected was approximately ∿0.1 of the total number of vacancies produced in the case of the 30 keV Cr^+ ion irradiation.

The most obvious physical reasons for the above discrepancy were as follows:

(1) It was only possible to examine a small fraction† (∿0.1 to 0.2) of the total tip volume (V_{tip}) in our search for SIAs, since only certain high-index planes were found to be satisfactory for detecting SIA contrast patterns (Beavan et al. 1971, Seidman and Lie 1972, Seidman 1973, Wei 1978).

(2) A fraction of the RCSs were propagated away from the DZs towards the irradiated surface; the upper limit to this fraction was less than 0.5. If the average value of the RCS range was greater than the distance of a DZ from the irradiated surface then some unknown fraction of these SIAs would have been shot out of the specimen. Figure 5 shows that only a few SIAs were detected in the half of the specimen which was exposed to the ion beam. Thus this reason also appears to be a very

---

† This value was estimated from the total number of atoms counted and the total number of atoms contained within V_{tip} examined. The quantity V_{tip} was given by:

$$V_{tip} = (\pi/3)\ (r_1^3 - r_o^3)\ (1-\sin\omega)^2/\sin\omega,$$

where r_o and r_1 were the initial and final radii of the tip and ω was the shank angle of the FIM specimen in the region of the tip.

plausible one.

(3) If the average RCS range was greater than the distance from a DZ to the unirradiated surface then many of the resulting SIAs could not have been detected. It was difficult to evaluate this possibility quantitatively since we did know a priori the average RCS range and the parent distribution of ranges of the SIAs which were deposited at the end of the RCS chains. Reasons (1) and (2) were sufficient to explain the fact that the fraction of SIAs detected was ~0.1 of the total number of vacancies produced. Thus there seems to be no compelling need to invoke reason number (3)--this point was discussed further in §5.2.

§5.2. The Distribution of Ranges of the Replacement Collision Sequences

In §§4.1 and 4.2 we presented distributions for the ranges of RCSs in tungsten FIM specimens, that had been irradiated with 18 keV Au^+ or 30 keV Cr^+ ions, along the $[\bar{7}4\bar{1}]$ direction; the value of $\langle R_{min} \rangle$ for these distributions was 175 ± (110-130) Å. The data in figs. 6 and 8 was combined with our earlier data* (Beavan, Scanlan and Seidman 1971) to produce the composite distribution exhibited in fig. 9; the value of $\langle R_{min} \rangle$ for this distribution was ≃160 ± 120 Å. To the best of our knowledge these are the only distributions (figs. 6, 8 and 9) of this type ever determined for RCSs.

The main problem with these range distributions was that we did not know the relationship between them and the parent standard distribution of RCS ranges. The problem was not simply a statistical one but rather a physical one because of the limitations of our sampling procedure (§5.1). Thus, for example, if a large number of SIAs in the immediate vicinity of each DZ had gone undetected, then our value of $\langle R_{min} \rangle$ would represent an overestimate of the mean range of RCSs. There was no plausible reason to believe that our $\langle R_{min} \rangle$ values underestimated the mean range of RCSs. The reason for this was that the fraction of SIAs per 50 Å bin (fig. 9) decayed

---

* In this research 25 SIAs were detected in a tungsten FIM specimen that had been irradiated at ≲18 K with 20 keV W^+ ions; the value of $\langle R_{min} \rangle$ was 81 ± 27 Å.

almost monotonically with distance from the DZs; whereas, one would expect the opposite behavior if a large fraction of the RCSs produced had traveled appreciable distances--along the close-packed crystallographic directions--without losing a significant fraction of their energy before they had come to rest as SIAs. It is noted, with respect to the latter point, that in the simulation of low-energy radiation damage events by the molecular dynamics technique no evidence was found for RCSs which travelled appreciable distances with very small energy losses to the lattice (Vineyard 1963, Erginsoy, Vineyard and Englert 1964, Tenenbaum 1978). Thus it is our opinion that the $\langle R_{min} \rangle$ values do not underestimate the mean range of RCSs but that they may overestimate it. The present distributions demonstrate that there were some RCSs with an appreciable range but the exact relationship between the measured fractions (see fig. 9) and absolute fractions of the parent standard distribution is unknown.

To quantify the above points, somewhat, concerning the ranges of RCSs we used the crude first-order focusing model--developed originally by Nelson and Thompson (1961) and Nelson (1963)--to estimate the focusing energies (E_f^{hkl}) and FCS ranges along different close-packed crystallographic directions in the b.c.c. lattice. The model of Nelson and Thompson assumed a repulsive Born-Mayer potential [$V_{W-W}(r)$] of the form:

$$V_{W-W}(r) = Ae^{-br} \qquad (1)$$

where r is the internuclear separation, A is a constant and b is the reciprocal of a screening length; we used A and b equal to 54,181 eV and 3.50171 Å^{-1}, respectively (Abrahamson 1969). The expressions for E_f^{hkl} were as follows (Nelson 1963):

$$E_f^{111} = 2A \exp\left(\frac{-\sqrt{3}}{4} a_o b\right), \qquad (2)$$

$$E_f^{110} = \frac{\sqrt{2}}{5}(a_o b)^2 A \exp\left(\frac{-\sqrt{5}}{4} a_o b\right) \qquad (3)$$

(in a {110} type plane)

and

$$E_f^{100} = 2A \exp\left(-\frac{1}{2} a_o b\right). \qquad (4)$$

The values of E_f^{111}, E_f^{110} and E_f^{100} calculated from eqns. (2) to (4)--employing a_o equal to 3.1648 Å--were 893, 383 and 425 eV, respectively. These values of E_f^{hkl} represent upper limits to this quantity and the real values may be at least a factor of two

smaller (for example, see Thompson 1969) for a "softer" interatomic potential. The corresponding maximum ranges of the FCSs were 86, 55 and 24 Å along the <111>, <110> and <100>-type directions, respectively; these values were calculated employing Nelson's (1963) expressions for the total number of collisions in a chain. The effect of zero point and thermal motion of the lattice atoms has been shown to decrease the maximum range of FCSs (for examples, see Nelson, Thompson and Montgomery 1962, Sanders and Fluit 1964 and Tenenbaum 1978). Thus, the above calculated values of the maximum ranges of FCSs would be further decreased by the inclusion of the zero point and thermal motions of the lattice atoms. In the case of our experiments the zero-point motion was the dominant effect because of the low irradiation temperatures (10 and <18 K) employed; the Debye temperature of tungsten is 310 K (de Launay 1956).

In a soft atomic collision one has the possibility of generating an RCS (Thompson 1969 and Nelson 1968). A simple analytical model of the replacement process suggested that the replacement energy (E_r^{hkl}) was equal to $E_f^{hkl}/4$ (Thompson 1969). An atom with an initial energy between E_f^{hkl} and E_r^{hkl} would generate an RCS, whereas one with an energy less than E_r^{hkl} would produce an FCS. The value of E_r^{hkl} determines the point in the RCS chain where the SIA is deposited and therefore the length of the chain. Thus one would expect the range of an RCS to be shorter than the range of an FCS. From all of the above it is clear that our experimental values of $\langle R_{min} \rangle$, in tungsten, could be almost a factor of ten greater than the calculated values of the RCS range. This discrepancy may be a result of inadequacies in the theoretical models of RCSs in a nonstatic lattice or, alternatively, in our sampling procedure as discussed earlier in this section.

§5.3 The Contribution of Focused or Replacement Collision Sequences to Sputtering

Current and Seidman (1980) and Current, Wei and Seidman (1980) have recently completed an extensive study of the sputtering of tungsten surfaces, at 10 K, employing the FIM technique. In this research they found that the number of vacancies detected in the near-surface region ($\lesssim$3 Å thick) of ion-irradiated specimens was approximately consistent with the continuum model of Sigmund (1969a and 1969b), for the average theoretical

sputtering yield [$S_{th}(\theta)$]; the quantity $S_{th}(\theta)$ represents the average number of atoms sputtered per projectile ion for a beam incident at an angle θ with respect to the normal to the surface being sputtered.

The result that the mean range of RCSs, in tungsten, may be as large as 160 ± 120 Å implies that the mean range of FCSs can have a comparable value. The intersection of an FCS with the surface of a specimen may cause a sputtered atom; a necessary condition is that the last atom in the FCS chain must have received an energy equal to the binding energy. An RCS can also result in a sputtered atom if its total chain length is greater than the distance from its site of creation to the surface of the specimen (e.g., see Thompson 1969 and 1978, Nelson 1968). A calculation of the exact contribution to the sputtering yield from DZs that do not have a portion of their volume in the near-surface region depends on a knowledge of the range distributions of both FCSs and RCSs. The interesting point for our results on tungsten is that we were able to obtain approximate agreement with the continuum sputtering model and also measure a mean range of RCSs that may be as long as 160 ± 120 Å.

ACKNOWLEDGEMENTS

We thank Mr. R. Whitmarsh for continued technical assistance and Dr. M.I. Current for a careful reading of the manuscript.

REFERENCES

Abrahamson, A.A., 1969, Phys. Rev., 178, 76.

Beavan, L.A., Scanlan, R.M., and Seidman, D.N., 1971, Acta metall., 19, 1339.

Blewitt, T.H., Kirk, M.A., and Scott, T.L., 1975, in Fundamental Aspects of Radiation Damage in Metals, edited by M.T. Robinson and F.W. Young, Jr. (Springfield, Virginia: National Technical Information Service), Vol. I, pp. 152-70.

Brinkman, J.A., 1954, J. Appl. Phys. 25, 961.

Current, M.I., and Seidman, D.N., 1980, Nuc. Instrum. Meth. 170, 377.

Current, M.I., Wei, C.-Y., and Seidman, D.N., 1980, Cornell Materials Science Center Report No. 4193, accepted for publication in the Philosophical Magazine.

Ecker, K.H., 1974, Rad. Effects, 23, 171.

Erginsoy, C., Vineyard, G.H., and Englert, A., 1964, Phys. Rev., 133, A595.

Erginsoy, C., Vineyard, G.H., and Shimuzu, 1965, Phys. Rev., 139, A118.

Gibson, J.B., Goland, A.N., Milgram, M., and Vineyard, G.H., 1960, Phys. Rev., 120, 1229.

de Launay, J., 1956, in Solid State Physics, edited by F. Seitz and D. Turnbull (New York: Academic Press), Vol. 2, p. 233.

Moore, A.J.W. and Nicholas, J.F., 1961, J. Phys. Chem. Solids, 20, 222.

Müller, E. W. and T.-T. Tsong, 1969, Field Ion Microscopy (New York: American Elsevier), pp. 119-127.

Nelson, R.S., 1963, Phil. Mag. 8, 693; 1968, The Observation of Atomic Collisions in Crystalline Solids (Amsterdam: North-Holland), pp. 188-241.

Nelson, R.S., and Thompson, M.W., 1961, Proc. Roy. Soc. A, 259, 458.

Nelson, R.S., Thompson, M.W., and Montgomery, H., 1962, Phil. Mag., 7, 1385.

Nicholas, J.F., 1965, An Atlas of Models of Crystal Surfaces, (New York: Gordon and Breach), pp. 110-111.

Park, J.Y., 1975, Ph.D. Thesis, Cornell University, Ithaca, New York.

Pétroff, P.M. and Seidman, D.N. 1973, Acta. metall., 21, 323.

Sanders, J.B., and Fluit, J.M., 1964, Physica, 30, 129.

Scanlan, R.M., Styris, D.L., Seidman, D.N., and Ast, D.G., 1969, Cornell University Materials Science Center Report No. 1159.

Scanlan, R.M., Styris, D.L. and Seidman, D.N., 1971a, Phil. Mag. 23, 1439; 1971b, Phil. Mag. 23, 1459.

Seeger, A., 1958, Proc. 2nd UN Int. Conf. Peaceful Uses of Atomic Energy, Geneva, Vol. 6, p. 250; 1962, Radiation Damage in Solids, (Vienna: IAEA), Vol. I, p. 101; 1970, Rad. Effects, 2, 165.

Seidman, D.N., 1973, J. Phys. F: Metal Phys., 3, 393; 1976, in Radiation Damage in Metals, edited by N.L. Peterson and S.D. Harkness, (Metals Park, Ohio: American Society for Metals), pp. 28-57; 1978, Surf. Science, 70, 532.

Seidman, D.N., and Lie, K.H., 1972, Acta metall., 20, 1045.

Seidman, D.N., and Scanlan, R.M., 1971, Phil. Mag. 23, 1429 (1971).

Seidman, D.N., Scanlan, R.M., Styris, D.L., and J.W. Bohlen, 1969, J. Phys. E: Scient. Instrum., 2, 473.

Seidman, D.N., Wilson, K.L., and Nielsen, C.H., 1975a, Phys. Rev. Lett. 35, 1041; 1975b, in Fundamental Aspects of Radiation Damage in Metals, edited by M.T. Robinson and F.W. Young, Jr. (Springfield, Virginia: National Technical Information Service), Vol. I, pp. 373-396.

Sigmund, P., 1969a, Phys. Rev., 184, 383; 1969b, Phys. Rev., 187, 768; 1980, in Sputtering by Ion Bombardment, edited by R. Behrisch (Berlin: Springer), in press.

Silsbee, R.H., 1957, J. Appl. Phys., 28, 1246.

Tenenbaum, A., 1978, Phil. Mag. A37, 731.

Tenenbaum, A., and Doan, N.V., 1977, Phil. Mag., 35, 379.

Thompson, M.W., 1969, Defects and Radiation Damage in Metals (Cambridge, England: Cambridge Press), pp. 188-239; 1978, in Physics of Ionized Gases: SPIG 1978 (Beograd, Yugoslavia: Institute of Physics), pp. 289-334.

Venables, J.A., 1970, in Atomic Collisions in Solids, edited by D.W. Palmer, M.W. Thompson and P.D. Townsend (Amsterdam North-Holland), pp. 132-161.

Vineyard, G.H., 1963, J. Phys. Soc. Japan, 18 (Suppl. III), 144.

Wei, C.-Y., 1978, Ph.D. Thesis, Cornell University, Ithaca, New York

Wei, C.-Y., Current, M.I., and Seidman, D.N., 1980, Cornell University Materials Science Center Report No. 4235.

Wei, C.-Y., and Seidman, D.N., 1978, Phil. Mag. A, 37, 257; 1979, Appl. Phys. Lett., 34, 622.

Whitton, J.L., 1973, in Channeling, edited by D.V. Morgan (New York: John Wiley), pp. 225-258.

Wilson, K.L., and Seidman, D.N., 1973, in Defects and Defect Clusters in B.C.C. Metals and Their Alloys, Nuclear Metallurgy edited by R.J. Arsenault (College Park Maryland: University of Maryland), Vol. 18, pp. 216-239; 1975, Rad. Effects, 27, 67.

Wilson, K.L., Baskes, M.I., and Seidman, D.N., 1980, Acta metall. 28, 89.

APPENDIX A

THE CRYSTALLOGRAPHY OF THE (521) PLANE

The crystallography of the (521) plane was not given in Nicholas' atlas (Nicholas 1965), hence we constructed a ball model of this plane employing the procedure developed by Moore and Nicholas (1961). Figure 10 exhibits a photograph of a ball model of the (521) plane, which was built on a (200) plane. The dark balls indicate the atoms in the outermost (zeroth) layer. The visible atoms--within the primitive mesh defined by the dark balls, O,A,B and C--from different layers are indicated by the numbers 1,2,3 and 4. The ball model was used to determine the primitive mesh and the stacking sequence of layers zero to four. Figure 11 exhibits the primitive mesh (plane zero) of the (521) plane and the positions of the atoms of planes 1 to 4 that project within the unit mesh. The vectors $\overrightarrow{OR} = (a_o/2)[0\bar{2}0]$, $\overrightarrow{OS} = (a_o/2)[\bar{1}11]$, and $\vec{w} = \overrightarrow{O1} = (a_o/2)[00\bar{2}]$ defined a primitive unit cell. The unit mesh exhibited in fig. 10 was shown from the ball model (fig. 9) to be determined by the vectors $\vec{u} = \overrightarrow{OA} = \overrightarrow{O1} - \overrightarrow{OS} = (a_o/2)\ [1\bar{1}\bar{3}]$ and $\vec{v} = \overrightarrow{OB} = \overrightarrow{O1} + \overrightarrow{OS} - \overrightarrow{OR} = (a_o/2)[\bar{1}3\bar{1}]$; the vectors $\vec{u}$, $\vec{v}$ and $\vec{w}$ also defined a primitive unit cell. The shift vector $\vec{t}$ which was the projection of $\vec{w}$ onto the zeroth layer of the (521) plane was given by $\vec{t} = \vec{w} - \vec{d}$, where the vector $\vec{t}$ was perpendicular to the (521) plane and had a magnitude equal to the spacing between (521) planes; for the (521) plane $\vec{d} = (a_o/3)[\bar{5}\bar{2}\bar{1}]$ and $\vec{t} = (a_o/30)[5\ 2\ 29]$. In fig. 10 $\vec{t}$ lies in the (521) plane; it connects the atom O with the projection of the atom 1 onto the zeroth layer of the (521) plane. The positions of atoms A,B and 1 to 4 relative to the cubic axes and O X Y Z were calculated following the approach developed by Nicholas (1965) and are listed in Table 2.

For a body-centered cubic lattice the number of planes in an identity period (N_{hkl}) is given by the equation $N_{hkl} = QQ^*(h^2 + k^2 + l^2)/2$ where Q is unity if h+k+l is odd and Q is 2 if h+k+l is even; Q* is 1 if h,k and l are all odd and Q* is 2 if h,k and l are of mixed parity. It is clear that one must use, in making this calculation, the Miller indices (hkl) before they have been converted into unmixed parity.

APPENDIX B

PROCEDURE FOR THE DETERMINATION OF THE POSITIONS OF THE SIAs AND DEPLETED ZONES IN AN FIM SPECIMEN

In this Appendix we describe the details of the procedure for determining the positions of the SIAs with respect to DZs in an FIM specimen. The end form of the FIM specimen was approximated by a hemisphere of initial radius r_o (see Fig. 12). As the specimen was successively field-evaporated atomic-layer by atomic-layer a final end-form with an average radius r_1 was obtained. The centers of the initial and the final hemispheres were denoted by the points O and O' respectively. From the FIM micrographs we knew the (hkl) plane and the number of the layer n in which a given SIA was detected; the value of n was measured from the initial surface. For example, an SIA at C was found in the nth layer of the $(h_4k_4l_4)$ plane measured from the initial surface at B. The problem was to determine the coordinates of point C given the quantities h_4, k_4, l_4 and n.

In fig. 11 we chose the ion beam direction to be parallel to the u-axis, the long axis of the specimen $[h_3k_3l_3]$ to be parallel to the w-axis and the vector $[h_2k_2l_2]$ as the v-axis. The vector $[h_2k_2l_2]$ was determined from the cross-product:

$$[h_2k_2l_2] = [h_3k_3l_3] \times [h_1k_1l_1]. \qquad \text{(B1)}$$

The u-, v-, w- axes and the origin O therefore constituted a rectangular coordinate system. The coordinates of point C were given by (u,v,w) in this rectangular coordinate system. The spherical coordinates (ρ,θ,ϕ) of point C are shown in fig. 11.

Initially, the center of the $(h_4k_4l_4)$ plane was at B. As a result of the specimen being pulse field evaporated the final location of the $(h_4k_4l_4)$ plane was at point D. In general, the vector $\vec{BD}$ was tilted away from the w-axis by an angle $\Delta\theta$. The angle $\Delta\theta$ was determined by analyzing the triangle BDF; point F was defined by the expression $|\overrightarrow{O'F}|=r_o$. The length $|\overrightarrow{AE}|$ was estimated by counting the number of layers (m) of the $(h_3k_3l_3)$ plane which were field-evaporated as the specimen reached its final end form; that is

$$g \equiv |\overrightarrow{AE}| = m d_{h_3k_3l_3}, \qquad \text{(B2)}$$

where the quantity $d_{h_3k_3l_3}$ is the interplanar spacing of the $(h_3k_3l_3)$ plane.

In the triangle BDF we have

$$|\vec{BF}| = |\vec{OO'}| = g + r_1 - r_o, \tag{B3}$$

$$|\vec{DF}| = r_1 - r_o, \tag{B4}$$

and

$$\measuredangle BFD = \theta_o. \tag{B5}$$

Hence the quantity $\Delta\theta$ was given by

$$\Delta\theta = \cos^{-1}\left[\frac{q^2 + (g+r_1-r_o)^2 - (r_1-r_o)^2}{2q\,(g+r_1-r_o)}\right], \tag{B6}$$

where the quantity q was given by

$$q=|\vec{BD}| = \sqrt{(r_1-r_o)^2+(g+r_1-r_o)^2-2(r_1-r_o)(g+r_1-r_o)\cos\theta_o}. \tag{B7}$$

The quantity θ_o, the angle between the normal vector $[h_4k_4l_4]$ of the $(h_4k_4l_4)$ plane and the w-axis, was given by

$$\theta_o = \cos^{-1}\left[\frac{h_3h_4 + k_3k_4 + l_3l_4}{\sqrt{h_3^2+k_3^2+l_3^2}\ \sqrt{h_4^2+k_4^2+l_4^2}}\right]. \tag{B8}$$

In the triangle BCO we have

$$|\vec{BO}| = r_o, \tag{B9}$$

$$\measuredangle CBO = \theta_o + \Delta\theta, \tag{B10}$$

and

$$s\equiv|\vec{BC}| = {}^{nd}h_4k_4l_4/\cos(\theta_o+\Delta\theta), \tag{B11}$$

where the quantity $d_{h_4k_4l_4}$ was the interplanar spacing of the $(h_4k_4l_4)$ plane. Therefore, the quantity ρ was given by

$$\rho \equiv|\vec{OC}| = \sqrt{s^2+r_o^2-2sr_o\cos(\theta_o+\Delta\theta)} \tag{B12}$$

and

$$\measuredangle COB = \cos^{-1}\left[\frac{r_o^2+\rho^2-s^2}{2r_o\rho}\right]. \tag{B13}$$

The angle θ was given by

$$\theta = \theta_o + \angle COB = \theta_o + \cos^{-1}\left(\frac{r_o^2+\rho^2-s^2}{2r_o\rho}\right) . \qquad (B14)$$

The projection of point B onto the u-v plane was denoted by point P. The vector $[h_5k_5l_5] \equiv \vec{OP}$ was therefore given by

$$\vec{OP} = \vec{OB} + \vec{BP}, \qquad (B15)$$

or

$$[h_5k_5l_5] = \frac{r_o}{\sqrt{h_4^2+k_4^2+l_4^2}}[h_4k_4l_4] - \frac{r_o\cos\theta_o}{\sqrt{h_3^2+k_3^2+l_3^2}}[h_3k_3l_3]. \qquad (B16)$$

Since the projection of the vector $\vec{OC}$ onto the u-v plane is parallel to the vector $[h_5k_5l_5]$, we obtained

$$\phi = \cos^{-1}\left[\frac{h_1h_5+k_1k_5+l_1l_5}{\sqrt{h_1^2+k_1^2+l_1^2}\ \sqrt{h_5^2+k_5^2+l_5^2}}\right] . \qquad (B17)$$

The spherical coordinates (ρ,θ,ϕ) of point C determined by eqs. (B12), (B14), and (B17) were transformed to the rectangular coordinates (u, v, w) according to the relationships:

$$u = \rho\sin\theta\cos\phi \qquad (B18)$$

$$v = \rho\sin\theta\sin\phi \qquad (B19)$$

and

$$w = \rho\cos\theta. \qquad (B20)$$

The rectangular coordinates (u,v,w) were finally transformed to the standard cubic coordinates (x, y, z). Thus, from eqs. (B1) to (B20) we calculated the rectangular coordinates (x, y, z) for any SIA by knowing the values of the quantities r_o, r_1, h_1, k_1, l_1, h_3, k_3, l_3, h_4, k_4, l_4, m and n; all these values obtained were from the analysis of FIM micrographs. The above computations were carried out with the aid of our NOVA 1220 minicomputer. The program for these computations was denoted DZP4 (Wei 1978) and is available upon request.

Table 1: Artifact vacancy concentrations detected in different vicinal planes near the (411) pole of unirradiated pure tungsten specimens

Plane	Number of atomic sites	Number of artifact vacancies	Artifact vacancy concentration (at.fr.)
{411}	68,582	24	3.5×10^{-4}
{521}	109,655	3	2.7×10^{-5}
{622}	41,815	337	8.0×10^{-3}
{631}	88,084	8	9.1×10^{-5}
{721}	71,143	42	5.9×10^{-4}
{732}	62,497	120	1.9×10^{-3}
{831}	104,074	8	7.9×10^{-5}
{842}	108,793	171	1.6×10^{-3}

Table 2: Table of atomic positions for the (521) plane of the bcc lattice

Atom	Co-ordinates of Position†								
	Relative to Cubic Axes			Relative to O X Y Z					
				$/\sqrt{11}$	$/\sqrt{330}$	$/\sqrt{30}$			
A	1	-1	-3	11	0	0	3.3166	0	0
B	-1	3	-1	-1	60	0	-0.3015	3.3029	0
1	0	0	-2	6	14	-2	1.8091	0.7707	-0.3651
2	-1	1	-1	1	28	-4	0.3015	1.5413	-0.7303
3	-1	1	-3	7	42	-6	2.1106	2.3120	-1.0954
4	-2	2	-2	2	56	-8	0.6030	3.0827	-1.4606

† The coordinates are given in terms of the length $a_o/2$, where a_o is the lattice parameter of the standard non-primitive unit cell. The coordinates relative to O X Y Z are given both in exact form and also numerically to four significant figures. The axis OX and OY are indicated in fig. 10 and OZ is the unit vector normal to the (521) plane.

FIGURE CAPTIONS

Figure 1: A schematic diagram of an (hkl) net plane. The solid black circles indicate normal lattice atoms and the numbered open circles vacant lattice sites (vacancies). The first ring of atoms of this net plane is indicated by the solid black line.

Figure 2: (a) A partial 121 stereographic projection illustrating the location of depleted zones (DZ5a to DZ5e) in the tungsten specimen which was irradiated, at 10 K, with 30 keV Cr^+ ions. The ion beam was parallel to the $[\bar{7}4\bar{1}]$ direction.

(b) A schematic cross-sectional view of the irradiated FIM specimen showing the relative positions of the DZs.

Figure 3: A series of 12 FIM micrographs out of 140 recorded during the atom-by-atom dissection of eight (732) planes. The contrast pattern of the SIA extended through six of these (732) planes. The positions of the atoms in the (732) planes are indicated schematically below each micrograph by solid black circles; a vacancy is indicated by an open circle.

Figure 4: A series of 12 FIM micrographs out of 581 recorded during the atom-by-atom dissection of nine (521) planes. The contrast pattern of the SIA extended through six (521) planes. The positions of the atoms and the vacancies in the (521) planes are indicated schematically below each micrograph; the symbols employed are the same as in Fig. (3).

Figure 5: A computer-generated isometric drawing showing the relative positions of the SIAs and DZ5a to DZ5e in a tungsten FIM specimen which was irradiated with 30 keV Cr^+ ions at 10 K. The open ellipses indicate DZs and the solid black circles indicate the SIAs.

Figure 6: The histogram of the number of SIAs per 50 Å bin versus R_{min} for the tungsten specimen which was irradiated with 30 keV Cr^+ ions at 10 K.

Figure 7: A computer-generated isometric drawing showing the relative positions of the SIAs (solid-black circles) in an FIM specimen which was irradiated with 18 keV Au^+ ions at 10 K; the ion beam was parallel to the $[\bar{7}4\bar{1}]$ direction. The locations of the DZs are indicated schematically by the open circles.

Figure 8: A histogram of the number of SIAs per 50 Å bin versus R_{min} for the tungsten specimen which was irradiated with 18 keV Au^+ ions at 10 K.

Figure 9: A composite histogram of the fraction of SIAs per 50 Å bin versus R_{min}, for the data presented in figs. 6 and 8 plus the data of Beavan, Scanlan and Seidman (1971) for a tungsten specimen which had been irradiated at ≤18 K with 20 keV W^+ ions.

Figure 10: A photograph of a ball model of the (521) plane built on a (200) plane. The dark balls indicate the atoms in the outermost (zeroth) layer. The visible atoms--within the primitive mesh defined by the dark balls O, A, B and C--from different layers are indicated by the numbers 1, 2, 3 and 4.

Figure 11: The primitive mesh (OABC) of the (521) plane and the projection of the atoms that lie within the primitive mesh for layers 1 to 4.

Figure 12: A schematic drawing of an FIM specimen illustrating how the coordinates of an SIA (or a DZ) at C within the specimen was determined; see Appendix B for the mathematical details.

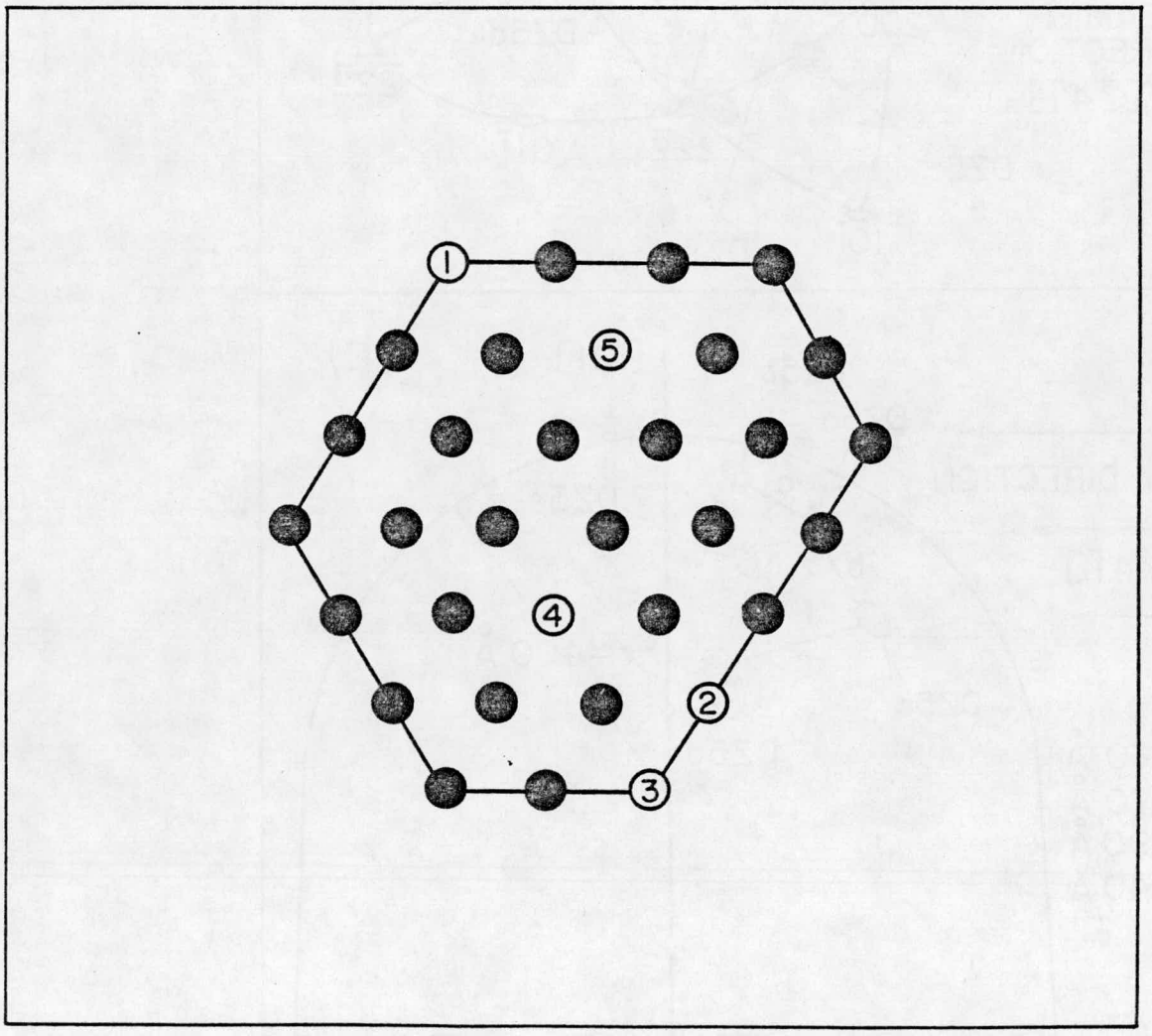

Figure 1

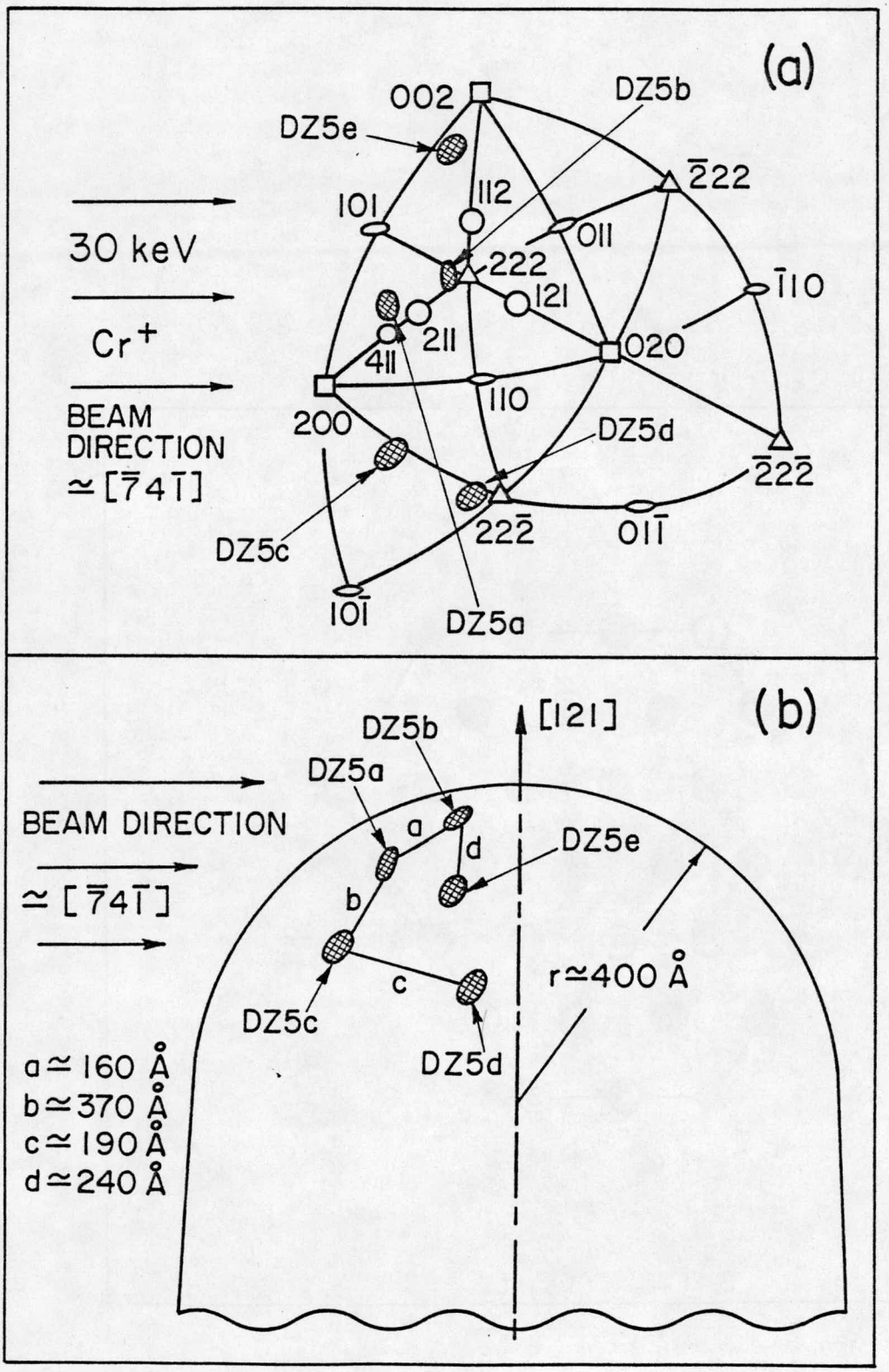
(a)
002
DZ5b
DZ5e
$\bar{2}22$
112
101
011
30 keV
222
$\bar{1}10$
121
Cr^+
211
020
411
110
BEAM
DIRECTION
≃[$\bar{7}4\bar{1}$]
200
DZ5d
$\bar{2}2\bar{2}$
$22\bar{2}$
$01\bar{1}$
DZ5c
$10\bar{1}$
DZ5a
(b)
[121]
DZ5b
DZ5a
BEAM DIRECTION
≃[$\bar{7}4\bar{1}$]
a
d
DZ5e
b
c
r≃400 Å
DZ5c
DZ5d
a≃160 Å
b≃370 Å
c≃190 Å
d≃240 Å

Figure 2

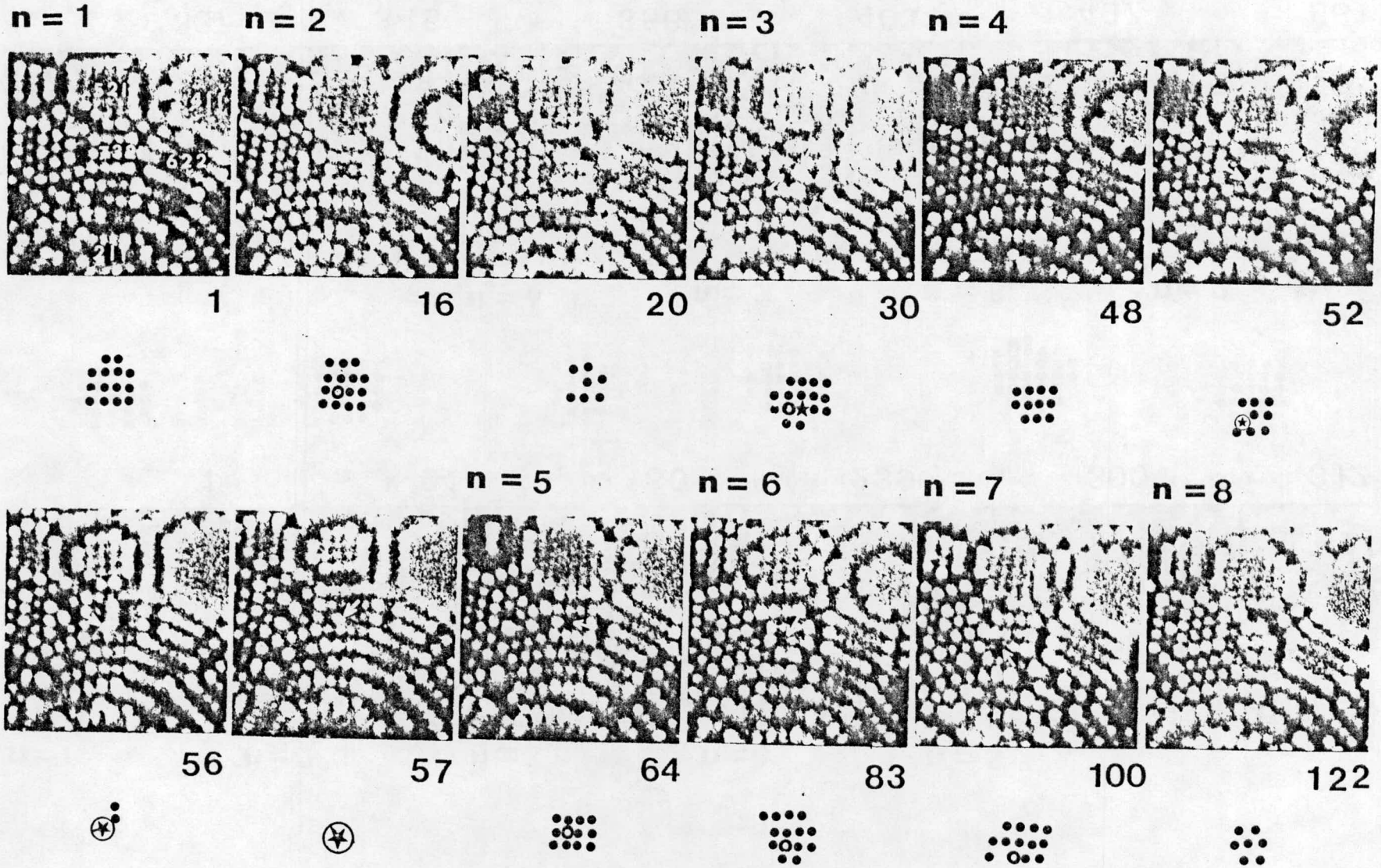

Figure 3

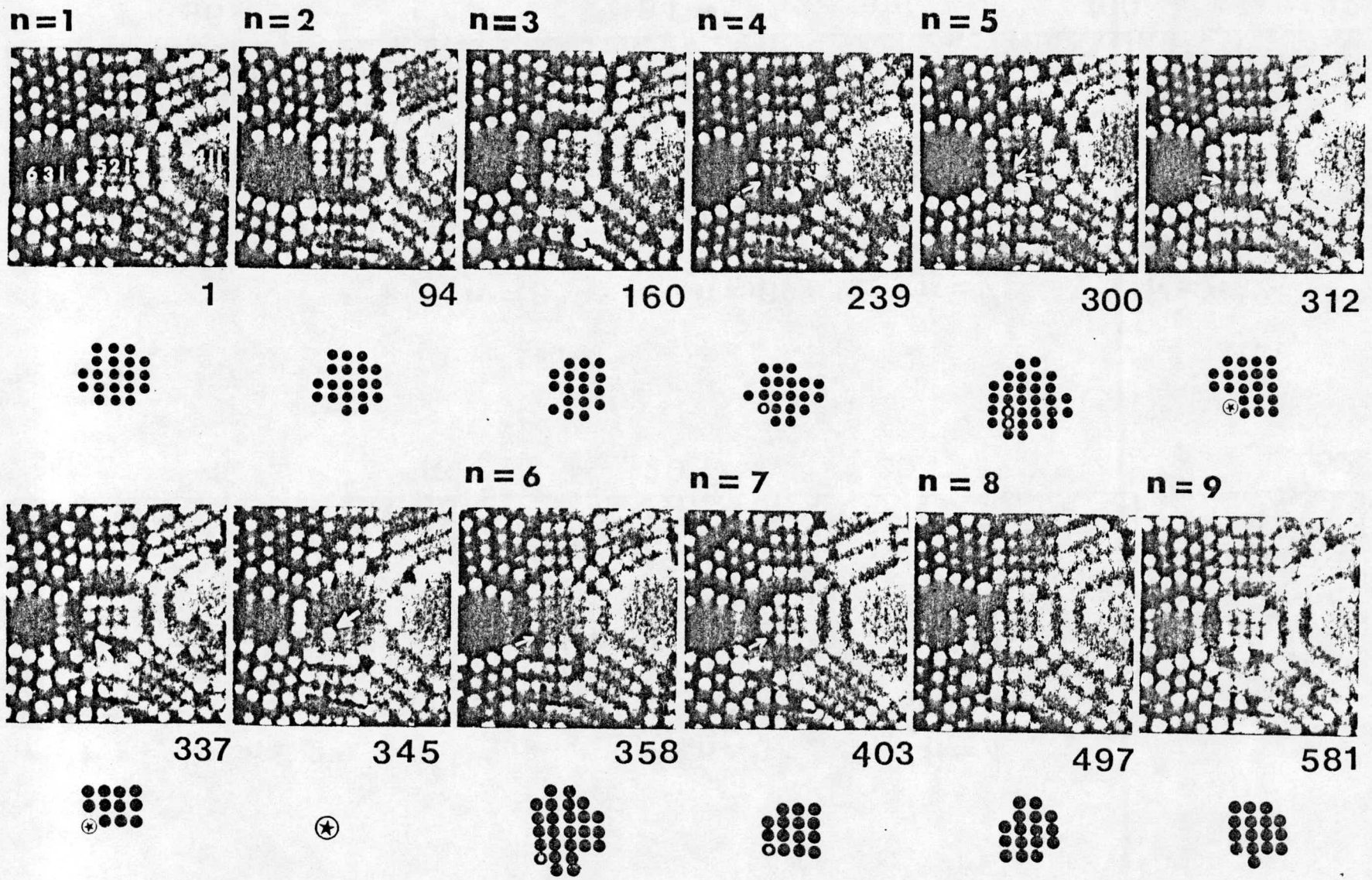
n=1
n=2
n=3
n=4
n=5
1
94
160
239
300
312
n=6
n=7
n=8
n=9
337
345
358
403
497
581

Figure 4

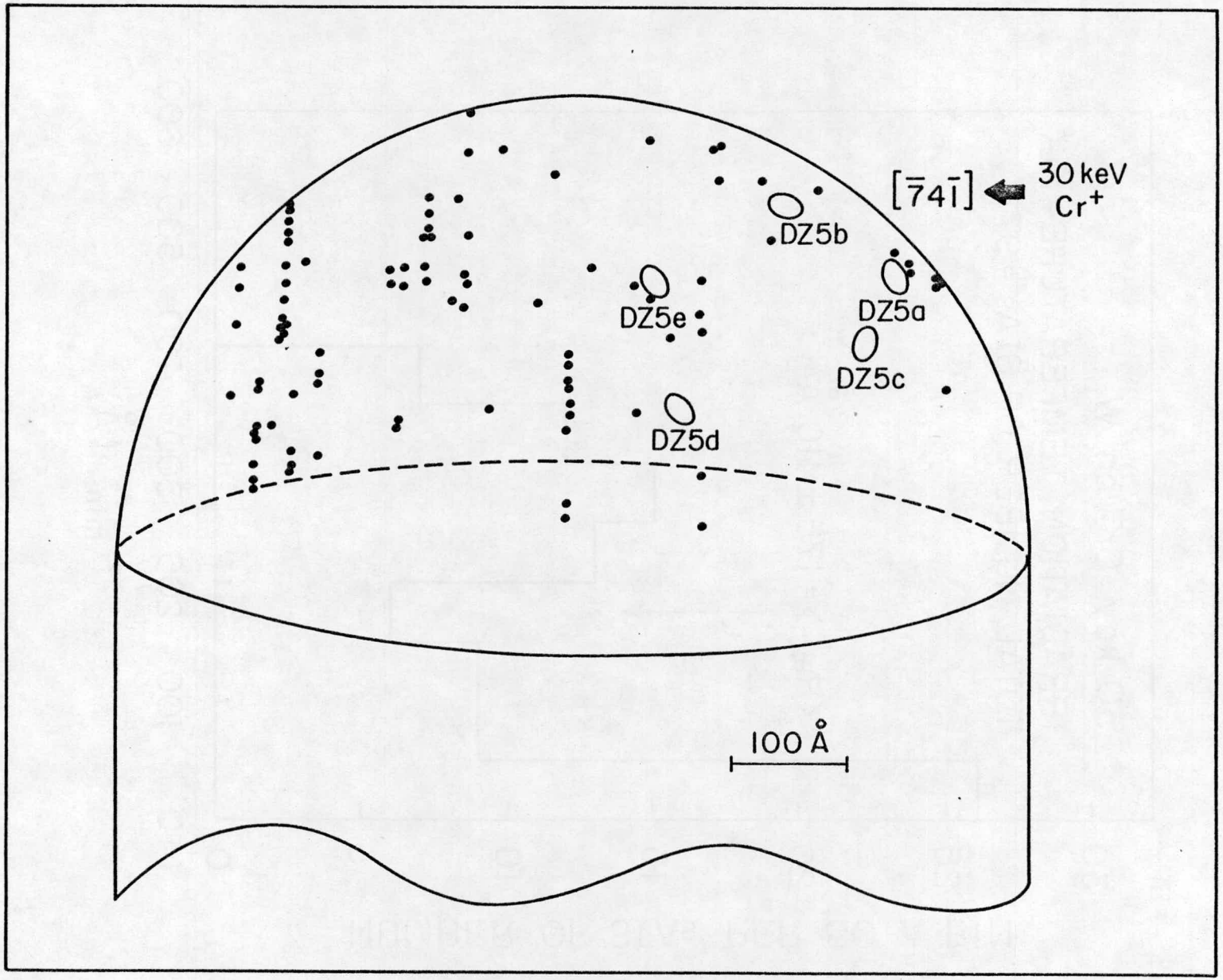

Figure 5

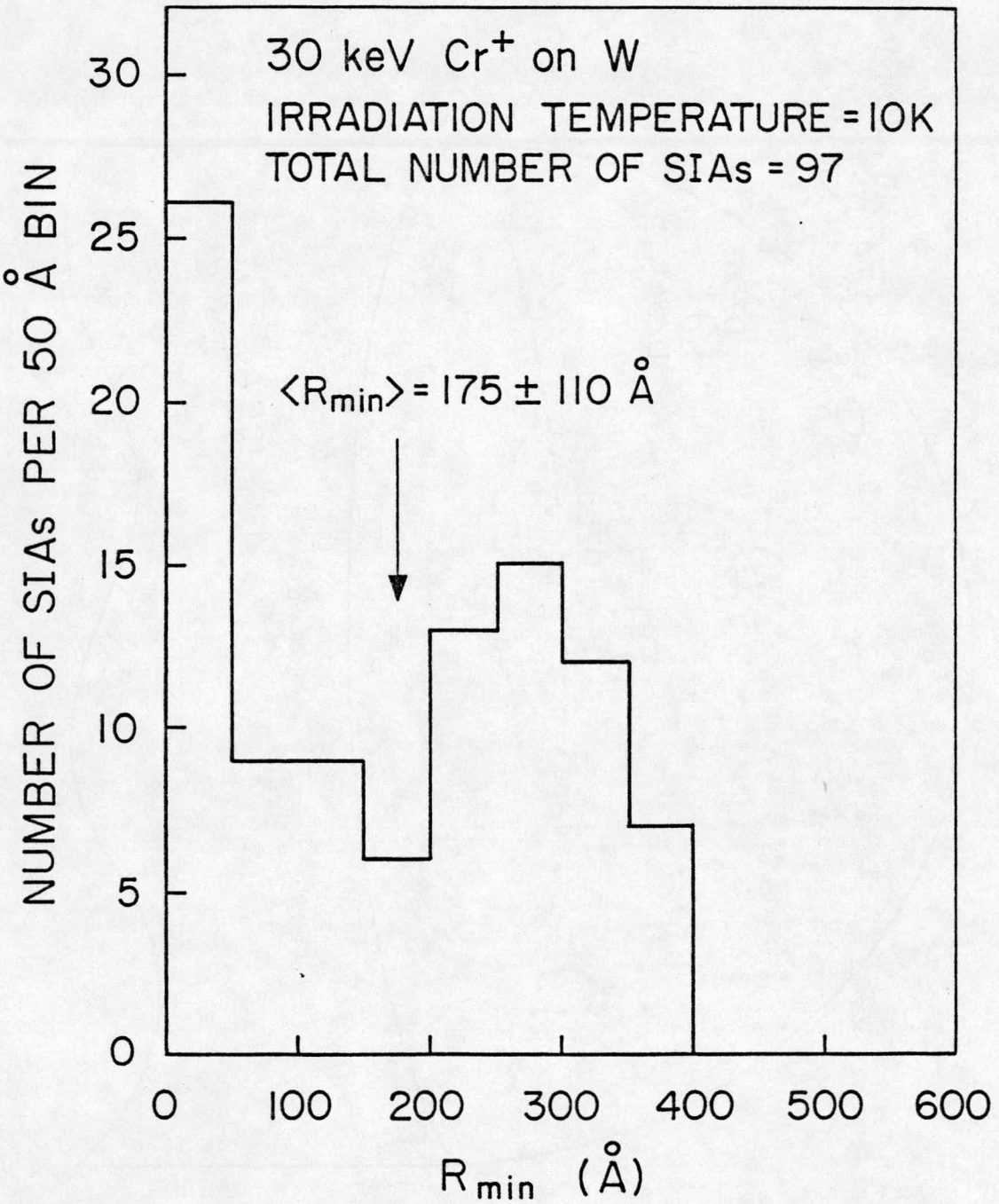
30 keV Cr+ on W
IRRADIATION TEMPERATURE = 10K
TOTAL NUMBER OF SIAs = 97
<Rmin> = 175 ± 110 Å
NUMBER OF SIAs PER 50 Å BIN
0
5
10
15
20
25
30
0
100
200
300
400
500
600
Rmin (Å)

Figure 6

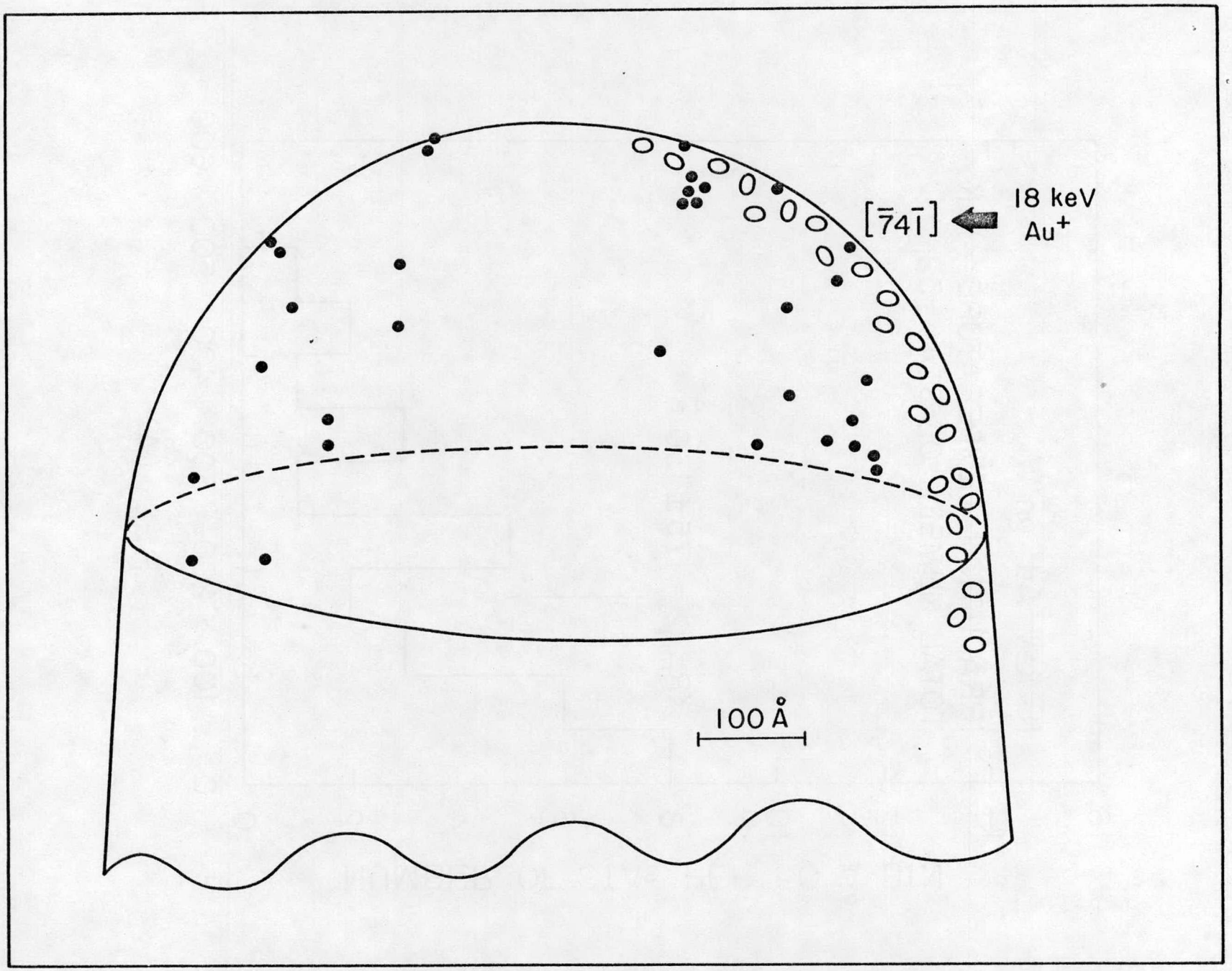

Figure 7

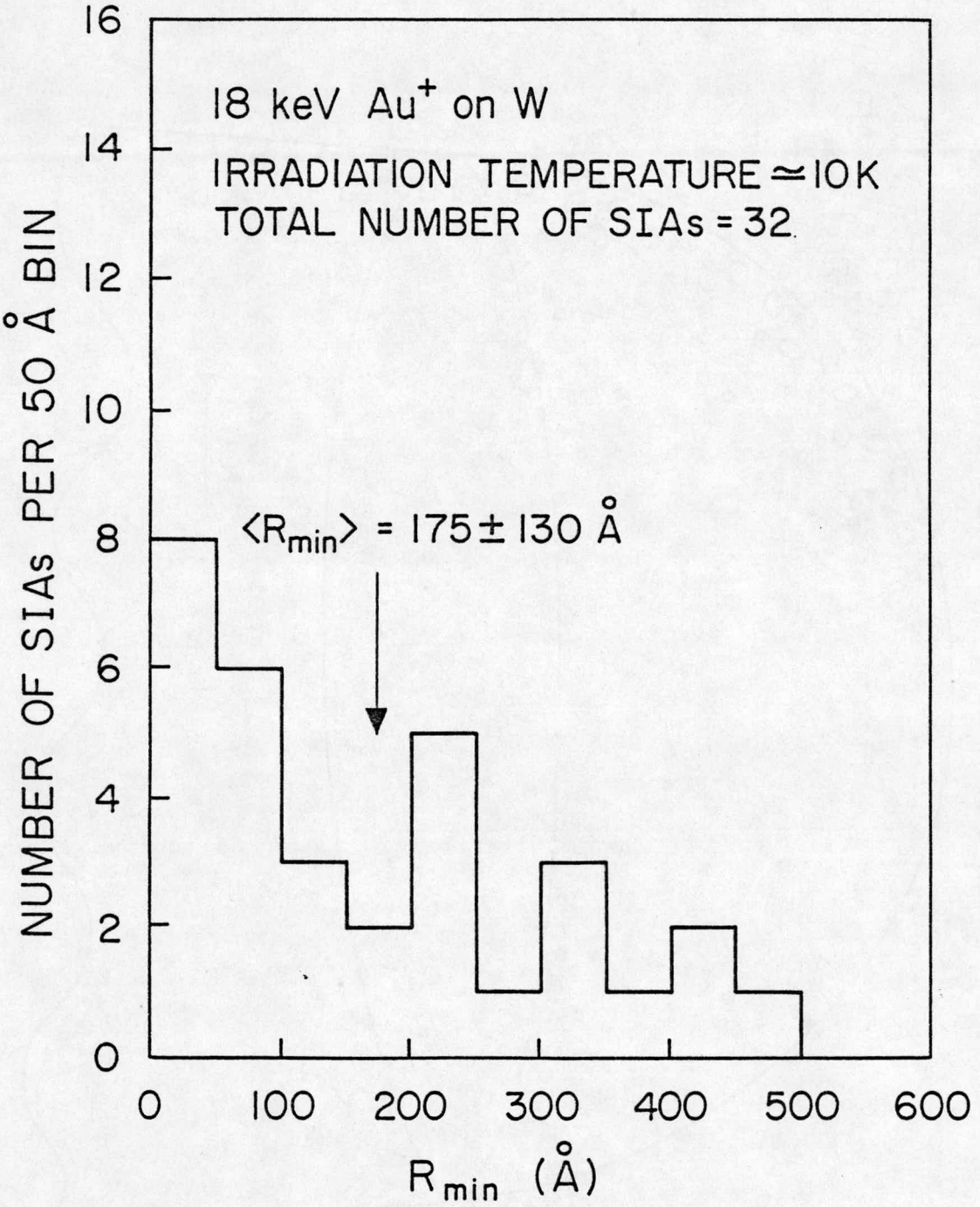
18 keV Au+ on W
IRRADIATION TEMPERATURE ≃ 10K
TOTAL NUMBER OF SIAs = 32
<Rmin> = 175 ± 130 Å
NUMBER OF SIAs PER 50 Å BIN
Rmin (Å)
0
2
4
6
8
10
12
14
16
0
100
200
300
400
500
600

Figure 8

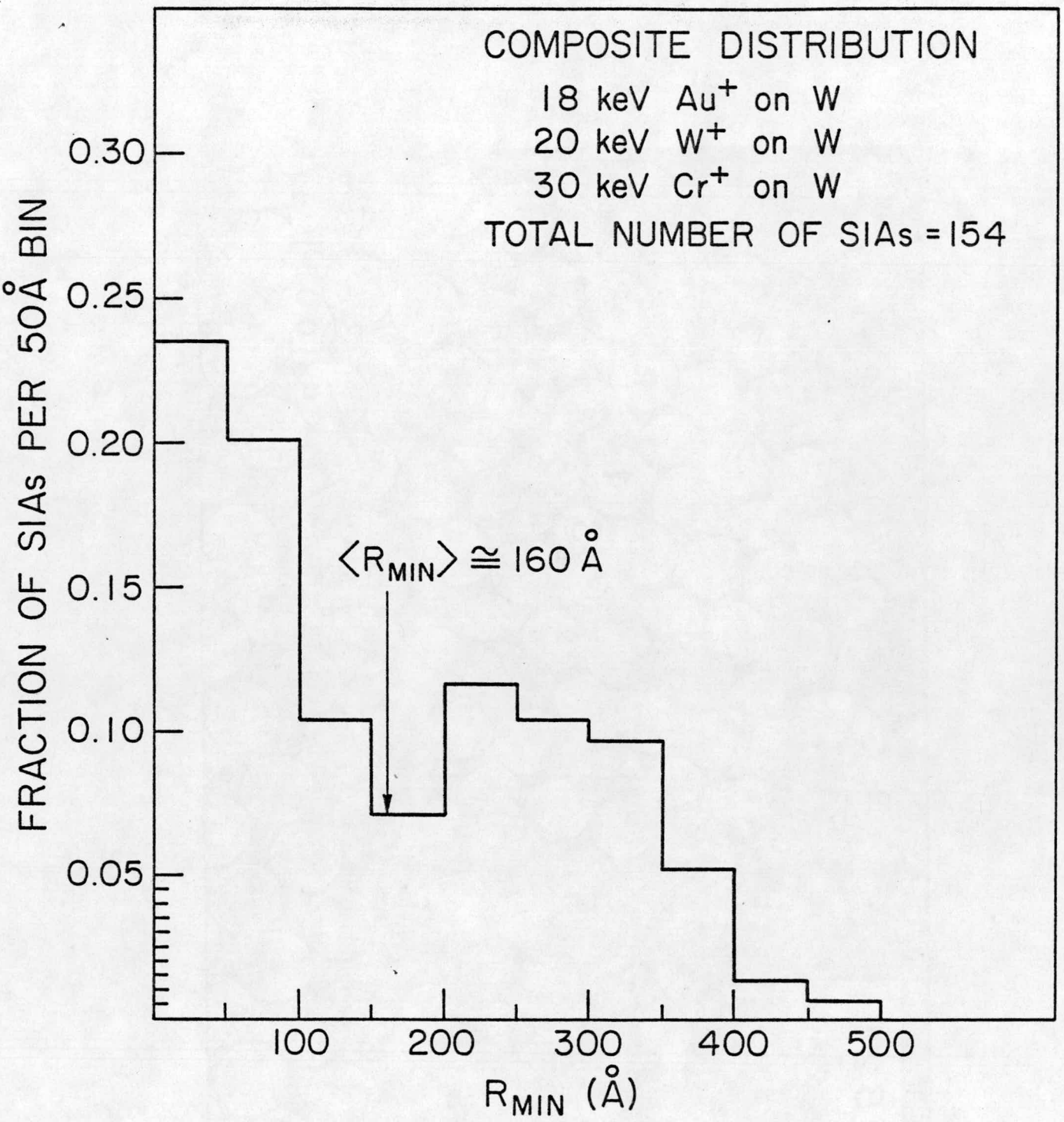
COMPOSITE DISTRIBUTION
18 keV Au+ on W
20 keV W+ on W
30 keV Cr+ on W
TOTAL NUMBER OF SIAs = 154
FRACTION OF SIAs PER 50Å BIN
0.30
0.25
0.20
0.15
0.10
0.05
⟨RMIN⟩ ≅ 160 Å
100
200
300
400
500
RMIN (Å)

Figure 9

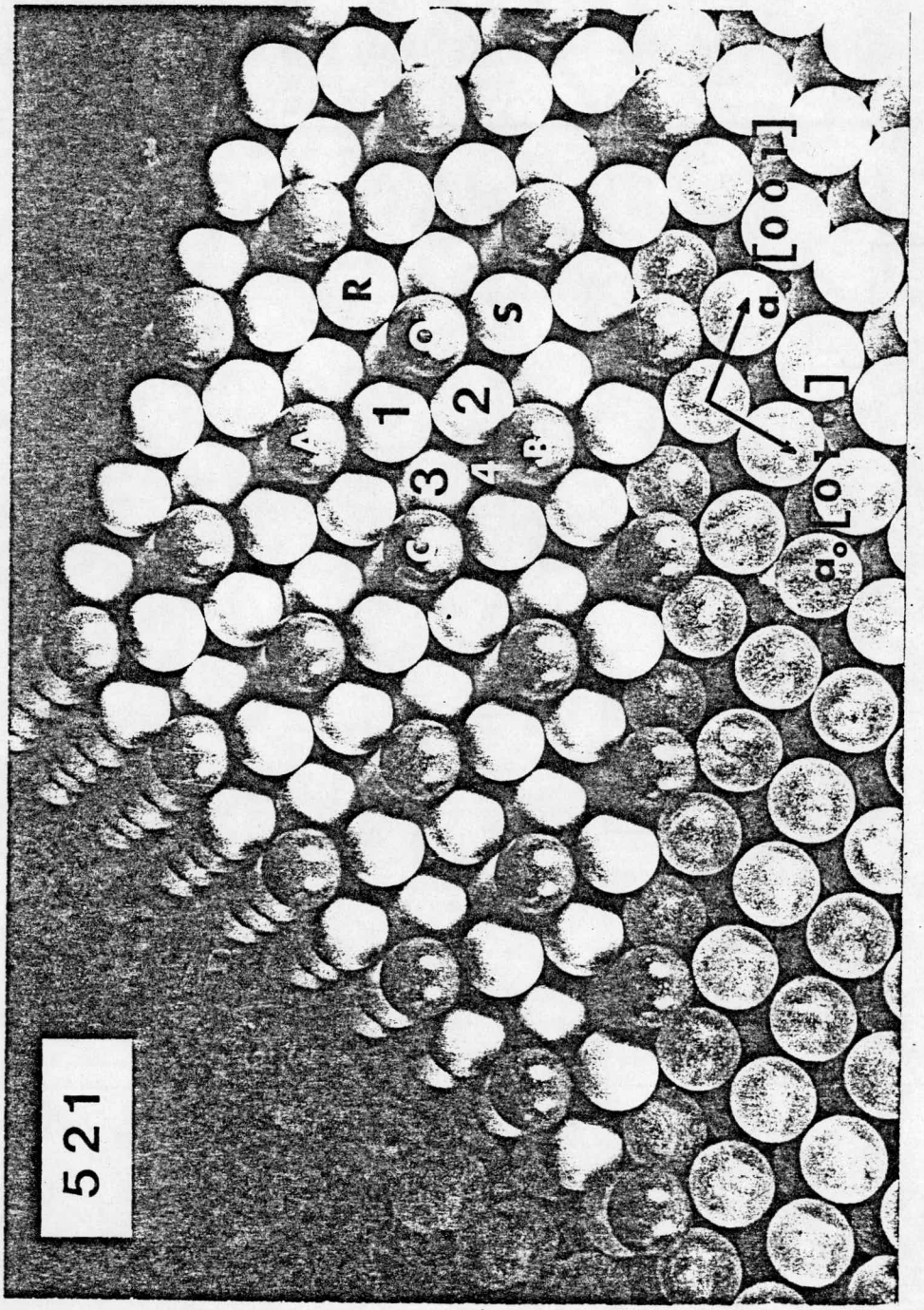

Figure 10

BCC (521)

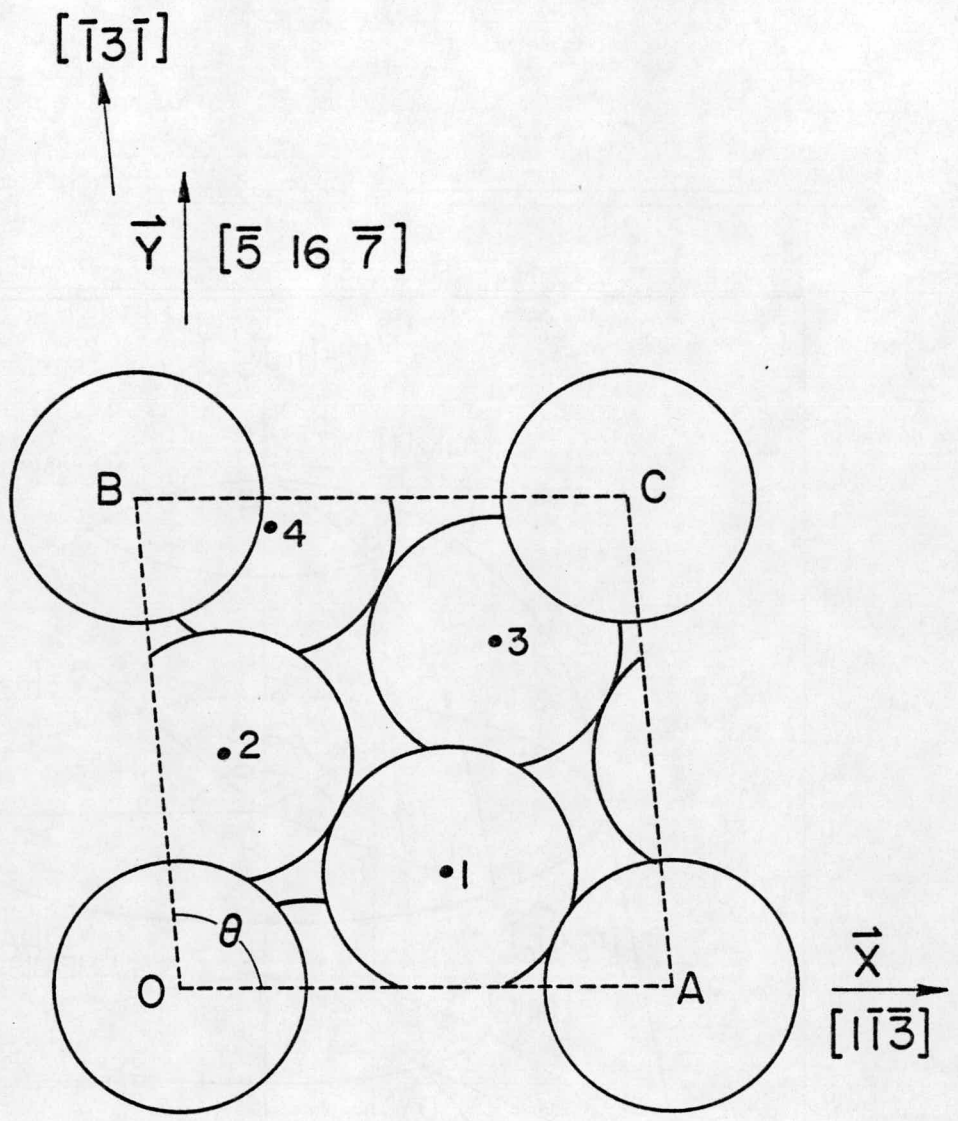

$\theta = 95.22°$

$\vec{u} = \overrightarrow{OA} = \frac{a_o}{2}[11\bar{3}]$

$\vec{v} = \overrightarrow{OB} = \frac{a_o}{2}[\bar{1}3\bar{1}]$

Figure 11

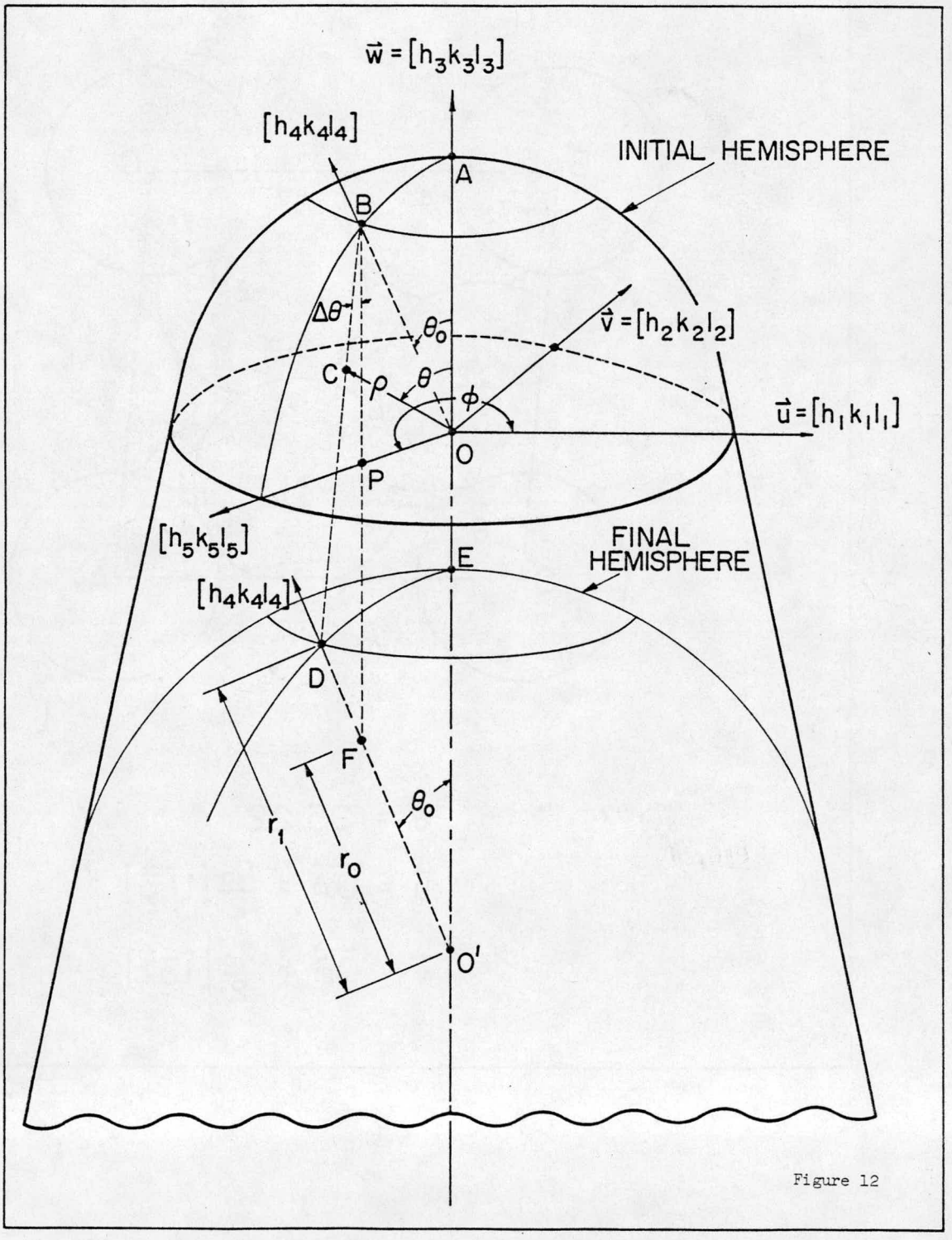
$\vec{w} = [h_3 k_3 l_3]$
$[h_4 k_4 l_4]$
INITIAL HEMISPHERE
A
B
$\Delta\theta$
θ_o
$\vec{v} = [h_2 k_2 l_2]$
C
ρ
θ
ϕ
$\vec{u} = [h_1 k_1 l_1]$
O
P
$[h_5 k_5 l_5]$
FINAL HEMISPHERE
E
$[h_4 k_4 l_4]$
D
F
θ_o
r_1
r_o
O'

Figure 12